ACS Sustainable Chemistry & Engineering

Research Article

pubs.acs.org/journal/ascecg

Solvothermal Synthesis of CeO_2–TiO_2 Nanocomposite for Visible Light Photocatalytic Detoxification of Cyanide

Chockalingam Karunakaran* and Paramasivan Gomathisankar

Department of Chemistry, Annamalai University, Annamalainagar 608002, Tamilnadu, India

ABSTRACT: A CeO_2–TiO_2 nanocomposite was synthesized solvothermally using ascorbic acid (A), urea (U), or polyvinylpyrrolidone (PVP). Powder X-ray and selected area electron diffractometries and Raman spectroscopy confirm the anatase phase of TiO_2 and face-centered cubic lattice of CeO_2. Energy dispersive X-ray spectroscopy confirms the purity of the synthesized composites and provides their compositions. Scanning electron, field emission scanning electron, and transmission electron microscopies give the sizes and shapes of the synthesized nanoparticles. UV–visible diffuse reflectance spectroscopy shows the optical absorption edges of CeO_2–TiO_2 (A), CeO_2–TiO_2 (U), and CeO_2–TiO_2 (PVP) as 510, 441, and 410 nm, respectively. The blue, blue-green, and green emissions shown by the three nanocomposites indicate the existence of defects such as oxygen vacancies in the crystal lattices. All three composites differ in their electrical properties, obtained by solid-state impedance spectroscopy. Furthermore, solid-state impedance spectroscopy shows photoconductance of CeO_2–TiO_2 confirming the band gap excitation by visible light. Under UV as well as visible light, the nanocomposite synthesized using ascorbic acid is the most efficient photocatalyst to detoxify cyanide in alkaline solution; the composite synthesized with urea is the least active photocatalyst. At neutral pH, CeO_2–TiO_2 synthesized with ascorbic acid is the most active to photocatalytically degrade dye, and the order of photocatalytic activity remains unaltered. The synthesized nanocomposites are not only photocatalysts but are bactericides as well. Ascorbic acid-assisted solvothermally synthesized CeO_2–TiO_2 is the most efficient bactericide, tested with *S. aureus* in the absence of direct light.

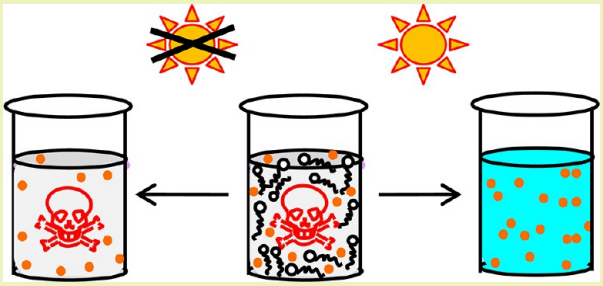

KEYWORDS: *Photocatalysis, Bacteria disinfection, Nanoparticles, Composite*

INTRODUCTION

The highly toxic cyanide ion is an effluent from electroplating and metal finishing shops. It is removed by physical, chemical, and biological treatments. While the physical methods only transfer the pollutant from one phase to another, biodegradation is a very slow process. The best available chemical treatment is alkaline chlorination, but it results in formation of highly toxic cyanogen chloride gas. Semiconductor photocatalysis is a promising method in which cyanide is mineralized by atmospheric oxygen through the formation of the cyanate intermediate, and reports on TiO_2 or ZnO-photocatalyzed cyanide oxidation with artificial UV light are many.[1−3] Visible light photocatalytic detoxification of cyanide is a sustainable method as it is driven by naturally available sunlight. Although reports on visible light photocatalytic mineralization of organics are many, those of cyanide are a few.[4,5] Some of the reasons are as follows. The carbon in the cyanide ion is more strongly bound to nitrogen than with atoms in dye molecules. The p*K*a of HCN is 9.3, and to avoid its volatilization, photocatalysis is to be carried out in a highly alkaline medium. This requires the photocatalyst to be stable in a highly basic medium. Furthermore, for effective photocatalysis, the substrate is to be adsorbed on the photocatalyst. In a basic solution, the semiconductor oxide surface is negatively charged due to adsorption of the hydroxide ion. This inhibits adsorption of the cyanide ion on the photocatalytic surface. So photocatalytic removal of cyanide is a tough job. Here, we present ascorbic acid-, urea-, and polyvinylpyrrolidone-assisted solvothermal synthesis of a CeO_2–TiO_2 nanocomposite to detoxify cyanide under visible light. TiO_2 and CeO_2 are stable in a basic medium and photocatalyze cyanide ion oxidation.[6] Sol–gel-prepared CeO_2/TiO_2 film[7] and CeO_2/TiO_2 nanoparticles obtained by mechanical grinding,[8] oil-in-water emulsion,[9] sol–gel,[10] solvothermal,[11] hydrothermal,[12,13] and precipitation[14] methods have been shown to degrade dye photocatalytically under visible light. Kinetics of the photodegradation of toluene by CeO_2–TiO_2 prepared by a microemulsion method has been studied.[15] Although some workers called the synthesized nanomaterials as Ce^{4+}-doped TiO_2,[7,9,11,12] the latter are more likely to be CeO_2–TiO_2 composites. The large size of Ce^{4+} hinders substitution of Ce^{4+} in the place of Ti^{4+} in the TiO_2 lattice, and the doped Ce^{4+} is likely to segregate to the surface of TiO_2 as CeO_2. Bacterial contamination of water is a potential health hazard demanding disinfection. Use of inorganic bactericides attracts interest because of their improved safety and stability.[16] Ceramics with inherent antibacterial activity are

Received: June 23, 2013
Revised: September 5, 2013
Published: September 6, 2013

   dx.doi.org/10.1021/sc400195n | *ACS Sustainable Chem. Eng.* 2013, 1, 1555−1563

convenient to employ because they are insoluble and easily recoverable. For the first time, our results show that the CeO_2−TiO_2 nanocomposite, besides serving as an efficient visible light photocatalyst to detoxify cyanide and mineralize organics, exhibits bactericidal activity. That is, it is a two-in-one bactericide and visible light photocatalyst that removes pollutants including cyanide.

EXPERIMENTAL METHODS

Solvothermal Synthesis. Polyvinylpyrrolidone (Himedia, 0.5 g) was dispersed in 20 mL of 2-propanol under sonication. For sonication, a Toshcon SW2 ultrasonic bath of 100 W at 37 ± 3 kHz was employed. Continuing sonication, ceric nitrate (Qualigens, 2 g) and 2 mL of titanium isopropoxide (Himedia) in 20 mL of 2-proponal was added drop by drop to get a yellowish solution. This was transferred into a Teflon-lined autoclave vessel and heated at 150 °C for 12 h. The solid was filtered, dried at 120 °C in a hot air oven for 3 h, and calcined at 500 °C for 2 h with the rate of heating as 10 °C min^{-1}. The sample is represented as CeO_2−TiO_2 (PVP). Similarly, CeO_2−TiO_2 (A) and CeO_2−TiO_2 (U) were synthesized using 2 g of ascorbic acid (Himedia) with 0.582 g of ceric nitrate and 2 g of urea (Sd fine) with 0.764 g of ceric nitrate, respectively, in place of polyvinylpyrrolidone.

Characterization. The powder X-ray diffraction (XRD) patterns were recorded with a PANalytical X'Pert PRO diffractometer using Cu Kα rays of wavelength 1.5406 Å in a 2θ range of 10−80° at a scan rate of 0.020° s^{-1}. The Raman system used was a WI Tec confocal micro Raman 300 R equipped with a liquid nitrogen-cooled detector. The excitation source was a He−Ne laser (633 nm) with a power of 2 mW on the sample. The laser was focused with a (50 × 100) long focal length objective to a spot of about 2 μm. Most of the measurements were made using a 300 g mm^{-1} grating and a confocal microscope with a 100 μm hole. The typical exposure time was 1 min. The spectrometer was calibrated by using the typical Si line at 520 cm^{-1}. JEOL JSM-5610 equipped with BE detector scanning electron microscope (SEM) was used to determine the morphology of the samples. The samples were placed on an adhesive carbon slice supported on copper stubs and coated with 10 nm thick gold dust using a JEOL JFC-1600 auto fine coater prior to measurements. Energy dispersive X-ray spectroscopic studies were also made with JEOL JSM-5610 SEM equipped with EDX. The field emission scanning electron microscopic (FE-SEM) images were obtained employing Hitachi SU6600. The materials, dispersed in methanol under sonication, were spread on aluminum foil placed on an adhesive carbon slice supported on a copper stub. The transmission electron microscopic (TEM) images were recorded with JEOL 100 CX 2. The samples were dispersed in acetone and spread on the grid for imaging. Formavar-coated copper grids were used for loading the samples. The selected area electron diffraction (SAED) patterns were also obtained with JEOL 100 CX 2. The diffuse reflectance spectra (DRS) were recorded using a PerkinElmer Lambda 35 spectrophotometer. The photoluminescence (PL) spectra were obtained with a PerkinElmer LS fluorescence spectrometer at room temperature. The nanocomposites were dispersed in carbon tetrachloride under sonication. The solid-state impedance spectra were recorded with a CH Instrument Electrochemical Analyzer 604C at room temperature in air over the frequency range from 0.1 MHz to 1 Hz. The disc area was 0.5024 cm^2, and the thickness of the CeO_2−TiO_2 (A), CeO_2−TiO_2 (PVP), and CeO_2−TiO_2 (U) pellets were 1.00, 0.57, and 0.63 mm, respectively.

Photocatalytic Study. Photocatalytic experiments with UV light were made with a multilamp photoreactor fitted with 8 W mercury lamps (Sankyo Denki, Japan) emitting at 365 nm. The light intensity was preserved by a highly polished anodized aluminum reflector. A borosilicate glass tube with a 15 mm inner diameter was used as the reaction vessel and was placed at the center. The cooling fans at the bottom of the reactor dissipate the generated heat. The light intensity was determined by ferrioxalate actinometry. An immersion type photoreactor with a 150 W tungsten halogen lamp fitted with a double-walled borosilicate immersion well with a 40 mm outer diameter with an inlet and outlet for circulation of $NaNO_2$ solution was used for visible light photocatalysis. A 2.0 M $NaNO_2$ solution removes 99% of the UV light with wavelengths between 320 and 400 nm and acts as a UV cut off filter. The light intensity (I) was measured using a Daystar solar meter (U.S.A.).

Solutions of cyanide of desired concentration at pH 12.5 were prepared fresh and used. The volume of the reaction solution was kept as 25 mL for UV photocatalysis and 75 mL for visible light photocatalysis. Air was bubbled through the reaction solution using a micro air pump that effectively stirred the solution and kept the suspended nanoparticles under continuous motion. The airflow rate was measured by the soap bubble method. The dissolved oxygen was determined using an Elico dissolved oxygen analyzer PE 135. The cyanide ion was estimated argentometrically using *p*-dimethylaminobenzylidene rhodamine as the indicator. The cyanide ion was also determined spectrophotometrically at 590 nm by complexing it with ninhydrin in alkaline medium. Cyanate was analyzed spectrophotometrically as reported already.[4] For the dye degradation experiment, an aqueous solution of rhodamine B of required concentration was prepared and used instead of a cyanide solution. Rhodamine B was estimated spectrophotometrically at 553 nm.

Bactericidal Study. A nutrient broth culture at pH 7.4 was prepared by dissolving 13.0 g of nutrient broth in 1 L of distilled water and sterilizing it in an autoclave at 121 °C. MacConkey agar plates were prepared separately by dissolving 55 g of MacConkey agar in 1 L of boiling distilled water followed by sterilization in an autoclave at 121 °C and pouring into a Petri dish. *Staphylococcus aureus* (*S. aureus*) bacteria were incubated in nutrient broth solution at 37 °C for 24 h under shaking. The cultured bacteria were centrifuged at 3500 rpm prior to washing. The treated bacteria were resuspended and diluted to about 1 × 10^7 CFU mL^{-1} with a 1.5% nutrient broth solution. The CFU was counted by a viable count method; 10 μL of the bacteria culture was streaked on the nutrient agar plate and incubated at 37 °C for 24 h. Twenty milligrams of the nanocomposite was added to 25 mL of the bacteria solution taken in a 60 mL bottle and shaken well continuously without any illumination. At the required time, a finite volume of the *S. aureus* solution was removed from the nanocomposite, streaked on agar plates, and enumerated.

RESULTS AND DISCUSSION

Crystalline Structure. The powder XRDs of CeO_2−TiO_2 (A), CeO_2−TiO_2 (U), and CeO_2−TiO_2 (PVP) are shown in Figure 1. The diffractograms display the XRD pattern of anatase TiO_2 (JCPDS card no. 89-4203) indicating its presence. Absence of rutile lines such as the 110 peak at 27.5° confirms

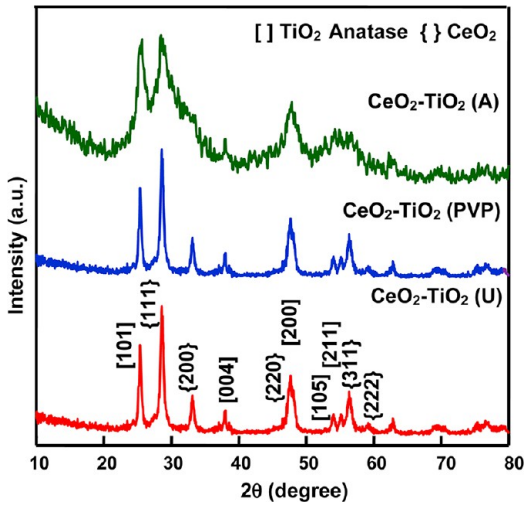

Figure 1. XRDs of solvothermally synthesized CeO_2−TiO_2 nanocomposites.

the absence of the rutile phase in the synthesized materials. Further, the presence of ceria in the synthesized samples is confirmed by the recorded XRDs. The 111, 200, 220, and 311 peaks of CeO_2 (JCPDS card no. 81-0792) confirm the presence of face centered cubic CeO_2. The absence of any other peaks indicates the synthesized materials as CeO_2−TiO_2 composites. The relatively wide XRD peaks of CeO_2−TiO_2 (A) shows formation of much smaller nanocrystals compared to the other two. The presence of the body-centered tetragonal anatase phase of TiO_2 and face-centered cubic phase of CeO_2 indicates segregation of the oxides during the crystal formation by solvothermal process. This is due to the large size of Ce^{4+}. The ionic radii of Ce^{4+} and Ti^{4+} are 0.97 and 0.64 Å, respectively, and hence, substitution of Ce^{4+} in place of Ti^{4+} in the TiO_2 lattice is difficult. As a result of the size mismatch between Ti^{4+} and Ce^{4+}, the cerium cation is largely concentrated at the surface, and grain boundaries of TiO_2 crystallites in the synthesized composites.

Raman spectra of CeO_2−TiO_2 (A), CeO_2−TiO_2 (U), and CeO_2−TiO_2 (PVP) are displayed in Figure 2. They confirm the

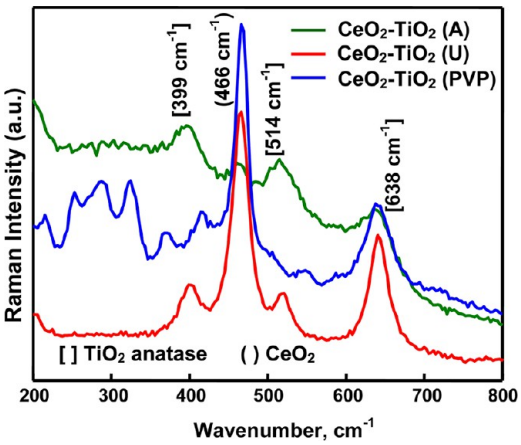

Figure 2. Raman spectra of CeO_2−TiO_2 nanocomposites.

presence of anatase TiO_2 in the synthesized samples. The peaks corresponding to B_{1g}, A_{1g}, and E_g modes of anatase TiO_2 are observed at 399, 514, and 638 cm^{-1}, respectively.[17−20] Furthermore, all three synthesized composites show a strong band at 466 cm^{-1}. This band is attributed to the vibrational mode of the F_{2g} symmetry of CeO_2, the only Raman-active mode of the perfect cubic fluorite lattice.[21−24] This indicates the presence of ceria in the composite. The F_{2g} peak is very strong in CeO_2−TiO_2 (PVP) and CeO_2−TiO_2 (U) but is weak in CeO_2−TiO_2 (A). The energy dispersive X-ray (EDX) spectra of the three composites are shown in Figure 3. They confirm the presence of cerium and titanium in the synthesized samples and also provide the composition. The percentage compositions of CeO_2 and TiO_2 in the ascorbic acid-, urea-, and polyvinylpyrrolidone-assisted solvothermally synthesized nanocomposites are 20.7 (Ce) and 79.3 (Ti), 21.2 (Ce) and 78.8 (Ti), and 42.1 (Ce) and 57.9 (Ti), respectively.

Morphology. The SEM images of CeO_2−TiO_2 (U) and CeO_2−TiO_2 (PVP) are presented in Figure 4. They reveal the fine particulate structure of the composites. The FE-SEM image of CeO_2−TiO_2 (A) is also displayed in Figure 4. It shows the nanoparticulate nature of CeO_2−TiO_2 (A). The particles are of spherical shapes with sizes between 10 and 15 nm and have agglomerated to take up a cauliflower-like structure. The TEM

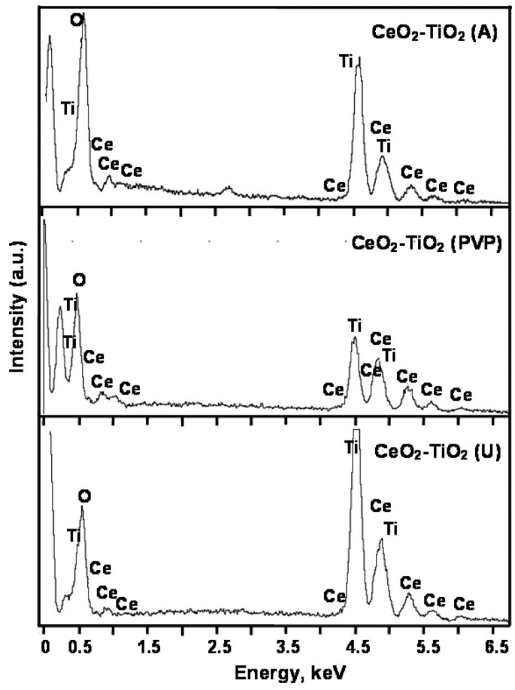

Figure 3. EDX spectra of CeO_2−TiO_2 nanocomposites.

image of CeO_2−TiO_2 (A) confirms the nanodimensions of the composite, and the particle size does not exceed 10 nm. The TEM images of all three synthesized composites are displayed in Figure 5. The TEM image of CeO_2−TiO_2 (U) shows the worm-like structure of the composite. The measured length and breadth are in the order of 80 and 30 nm, respectively. The CeO_2−TiO_2 (PVP) nanoparticles appear to be cuboids, and the recorded TEM image shows the diagonal of the cuboids between 8 and 25 nm. The selected area electron diffraction (SAED) patterns of all the three composites are displayed in Figure 6. They clearly reveal the presence of anatase TiO_2 and cubic CeO_2; the 101 plane of anatase TiO_2 and 111 plane of cubic CeO_2 are seen through their interplanner spacing. These results are in total agreement with the observed XRDs.

Optical Properties. The diffuse reflectance spectra (DRS) of the nanocomposites are shown in Figure 7. The reflectance data, reported as $F(R)$ values, have been obtained by the application of the Kubelka−Munk (K-M) algorithm. The DRS of CeO_2−TiO_2 (A) shows strong visible light absorption. The band gaps of the synthesized nanocomposites have been deduced from the modified K-M plots. Figure 8 is the plots of $[F(R)h\nu]^{1/2}$ versus photon energy. The extrapolation of $[F(R)h\nu]^{1/2}$ to the abscissa at zero $F(R)$ provides the band gap energies of CeO_2−TiO_2 (A), CeO_2−TiO_2 (U), and CeO_2−TiO_2 (PVP) as 2.43, 2.81, and 3.09 eV, respectively, and the values correspond to absorption edges of 510, 441, and 410 nm, respectively. The measured reflectance data of the composites fit more satisfactorily the $[F(R)h\nu]^{1/2}$ versus photon energy plot than the $[F(R)h\nu]^2$ versus photon energy plot suggesting a strong indirect band gap transition.

Figure 9 displays the photoluminescence spectra of the synthesized nanocomposites. The nanocrystals were suspended in carbon tetrachloride by sonication and excited at 350 nm. The spectra mainly consist of four emission bands: a blue band at 420 nm (2.95 eV), which is weak in CeO_2−TiO_2 (A) but moderately strong in CeO_2−TiO_2 (U) and CeO_2−TiO_2 (PVP), a blue band at 462 nm (2.68 eV), a strong blue-green

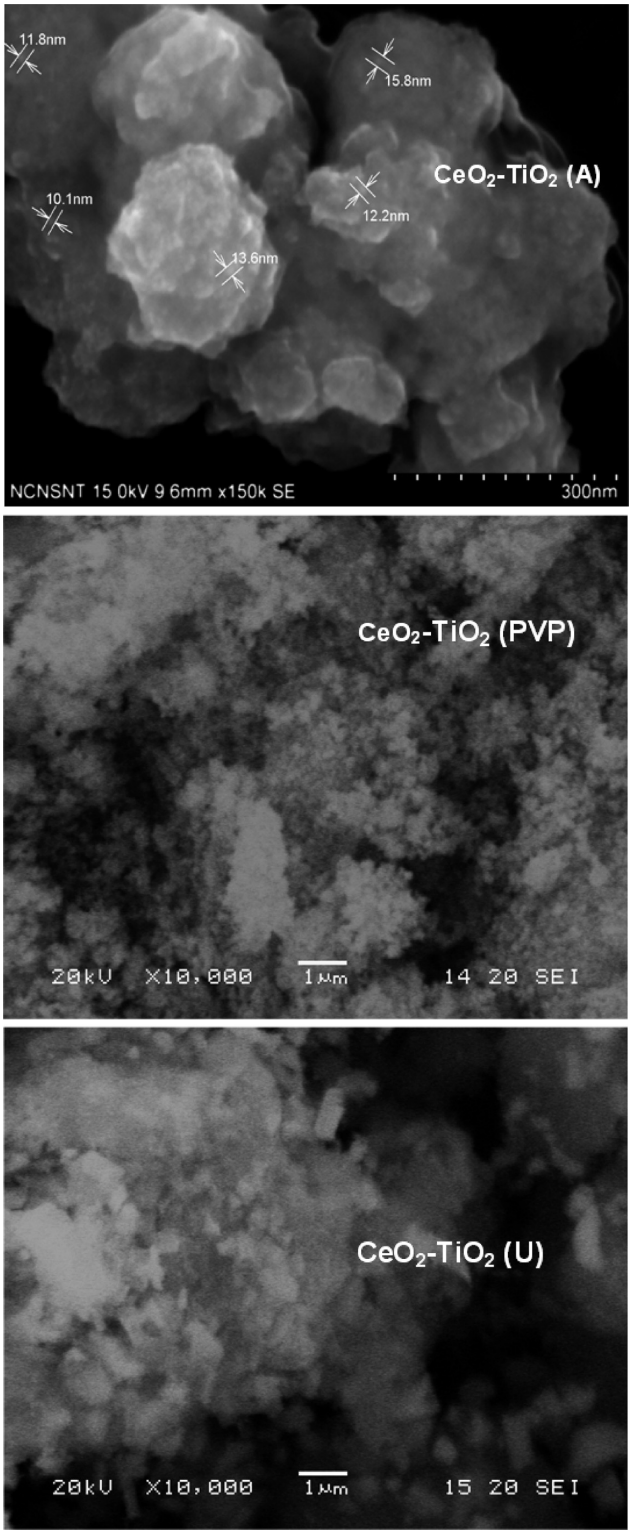

Figure 4. SEM images of CeO_2−TiO_2 nanocomposites.

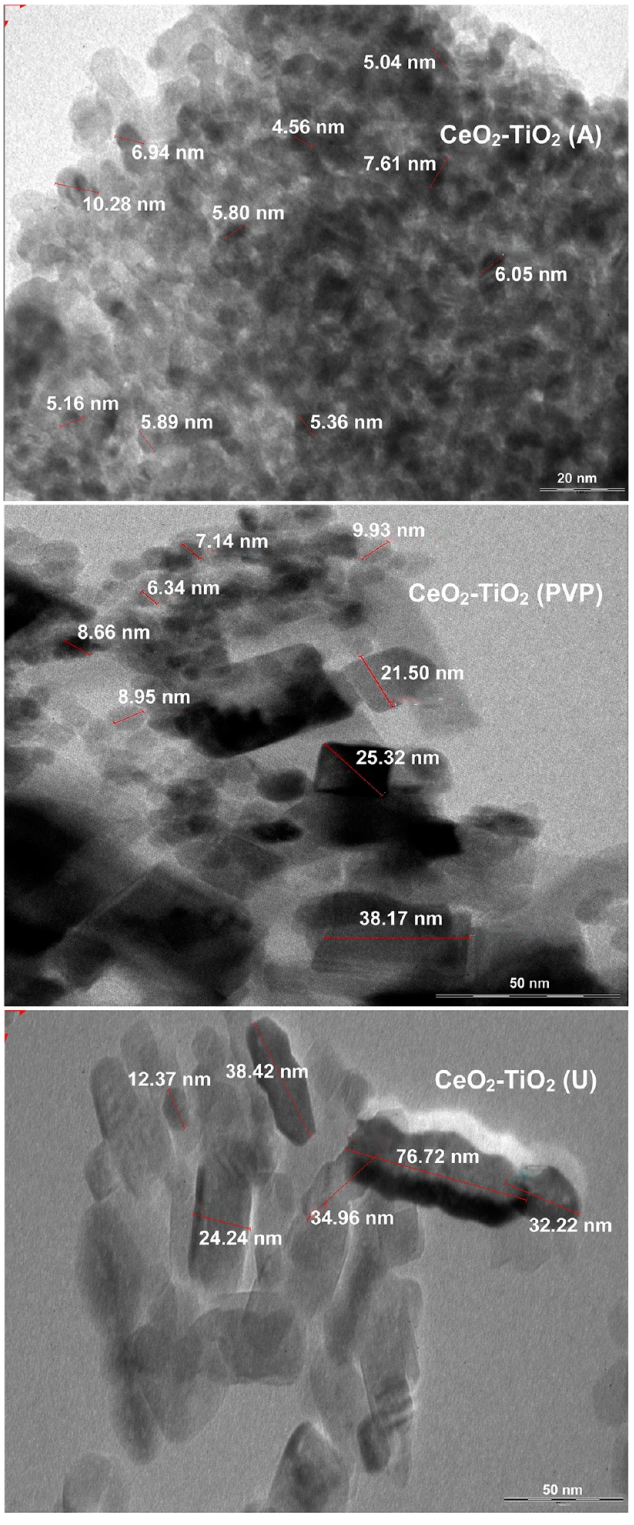

Figure 5. TEM images of CeO_2−TiO_2 nanocomposites.

band at 482 nm (2.57 eV), and a weak green band at 527 nm (2.35 eV). The two peaks at 482 and 527 nm may be due to the TiO_2 phase.[25] They are attributed to the transition from the oxygen vacancies with two trapped electrons and one trapped electron to the valence band of TiO_2, respectively. The energy levels related to the two kinds of the oxygen vacancies are located at 0.51 and 0.82 eV below the conduction band (CB) of TiO_2, respectively. Because of the existence of the energy levels of oxygen vacancies, first the photogenerated electrons in the CB is likely to reach the oxygen vacancies through a non-radiative process and then recombine with the photogenerated holes in the valence band (VB) accompanied by the emission of fluorescence. The observed broad band at 440−560 nm (2.20−2.80 eV) in the visible region is also ascribed to the radiative recombination of excitons of the shallow traps identified with oxygen vacancies and Ti^{4+} adjacent to oxygen vacancies.[19] The weak blue (420 nm) and strong blue-green (462 and 482 nm)

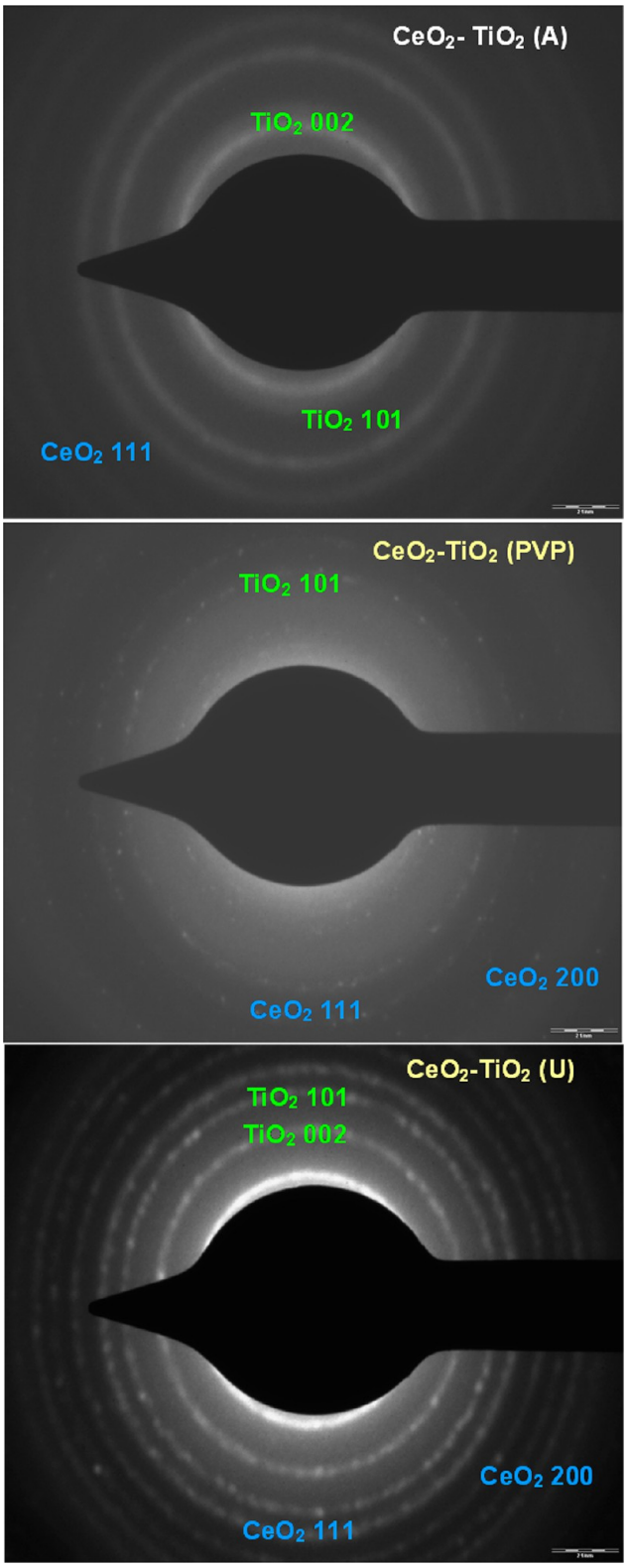

Figure 6. SAEDs of CeO_2−TiO_2.

emissions may be attributed to surface defects in the CeO_2 phase, and the low intensity of the green emission (527 nm) may also be due to the low density of oxygen vacancies in the CeO_2 lattice.[26] Furthermore, examination of the near band gap emission, NBE (420 nm), and deep level emission, DLE (482 nm), of the synthesized composite shows suppression of NBE

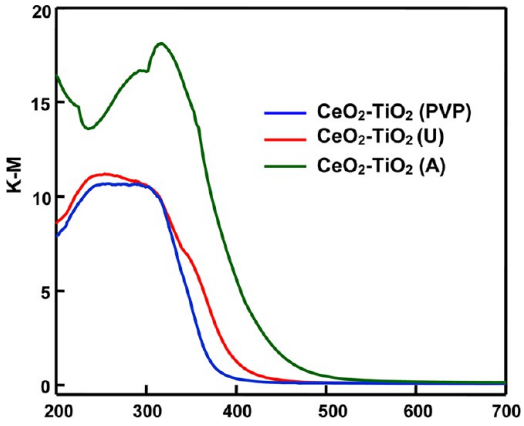

Figure 7. Diffuse reflectance spectra of CeO_2−TiO_2 nanocomposites.

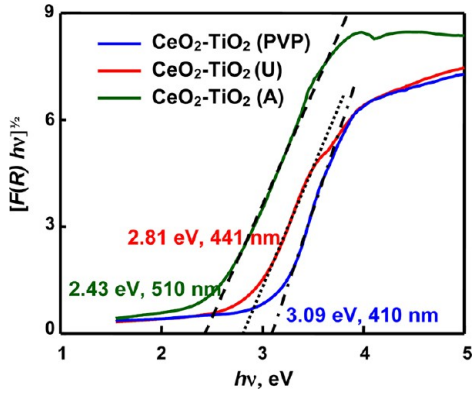

Figure 8. Modified K-M plots.

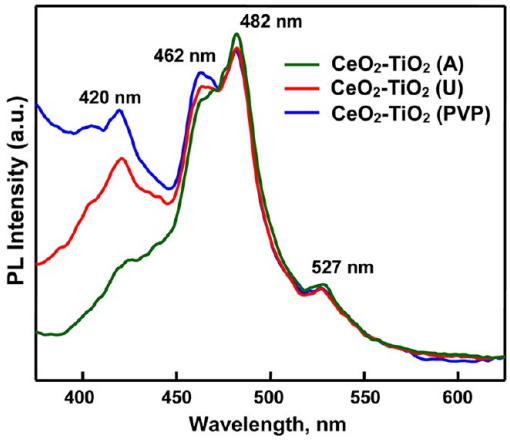

Figure 9. Photoluminescence spectra of CeO_2−TiO_2 nanocomposites.

when using ascorbic acid instead of urea or PVP as the templating agent in the solvothermal synthesis. The ratio of intensity of DLE to that of NBE reflects the extent of defect, and the ratios, respectively, are 3.3, 1.6, and 1.2 for using ascorbic acid, urea, and PVP as templating agents. These ratios indicate that a lattice defect is more pronounced in CeO_2−TiO_2 obtained using ascorbic acid than using urea or PVP. The main reason responsible for suppression of NBE or enhancement of DLE is a decrease in the crystallinity of the synthesized nanocomposite. DLE is related to structural defects,[27] and the crystalinity is decreased when using ascorbic acid instead of employing urea or PVP. This finds support from the recorded XRDs (Figure 1).

dx.doi.org/10.1021/sc400195n | ACS Sustainable Chem. Eng. 2013, 1, 1555−1563

Electrical Properties. Measurement of solid-state impedance in the frequency range from 0.1 MHz to 1 Hz reveals a decrease in impedance with increase in frequency indicating the capacitance of all the synthesized CeO_2−TiO_2 nanocomposites. Figure 10 presents the Nyquist plots. The Nyquist plots of

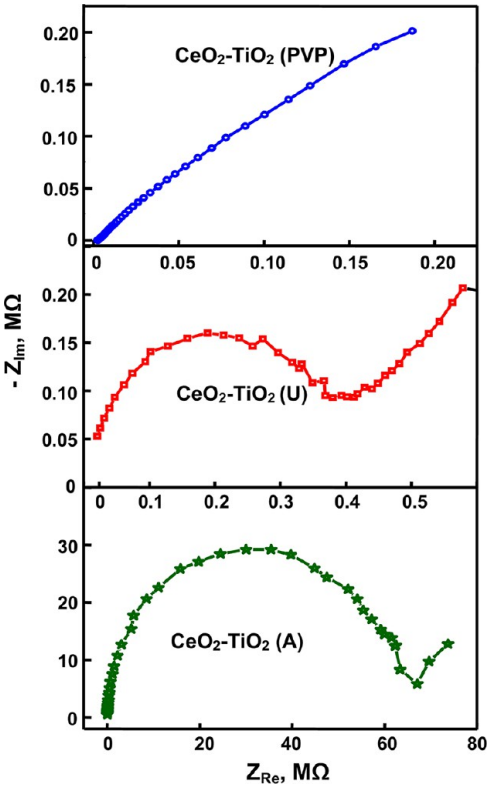

Figure 10. Solid-state impedance spectra.

CeO_2−TiO_2 (A) and CeO_2−TiO_2 (U) are semicircular indicating the uniform distribution of CeO_2 on TiO_2. The specific conductance (σ), capacitance (C), and charge−transfer (R_{CT}) resistances of CeO_2−TiO_2 (A) and CeO_2−TiO_2 (U) are 0.30 and 36 μS m^{-1}, 3.7 and 37.8 pF, and 67.0 and 0.36 MΩ, respectively. The specific conductance and capacitance of CeO_2−TiO_2 (U) are much larger than those of CeO_2−TiO_2 (A). However, CeO_2−TiO_2 (PVP) does not exhibit the characteristic semicircular arc but displays a linear variation of $-Z_{Im}$ with Z_{Re}, which is characteristic of a diffusion-controlled process. This may be because of the high percentage composition of CeO_2 in the composite.

Optoelectrical Properties. Band gap illumination of the semiconductor promotes electrons from VB to CB. This should reflect the conductance of the semiconductor under illumination. Figure 11 presents the Nyquist plots of CeO_2−TiO_2 (A) illuminated with visible light using a tungsten halogen lamp. The corresponding plots in the absence of illumination are shown for comparison. The plots reveal the decrease in charge−transfer resistance on illumination with visible light and thus confirm band gap excitation of CeO_2−TiO_2 (A) by visible light.

Photocatalytic Detoxificatation of Cyanide. Figure 12 shows the time profiles of cyanide oxidation catalyzed by CeO_2−TiO_2 nanocomposites under visible light, illuminated by a tungsten halogen lamp. $NaNO_2$ (2 M) solution used to cool the tungsten lamp acts as a UV light cutoff filter; it removes

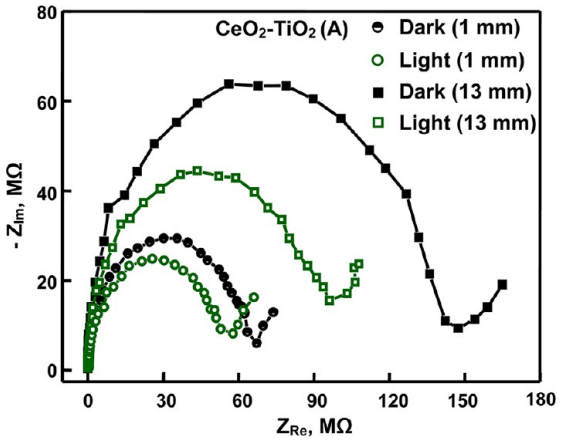

Figure 11. Nyquist plots with and without illumination.

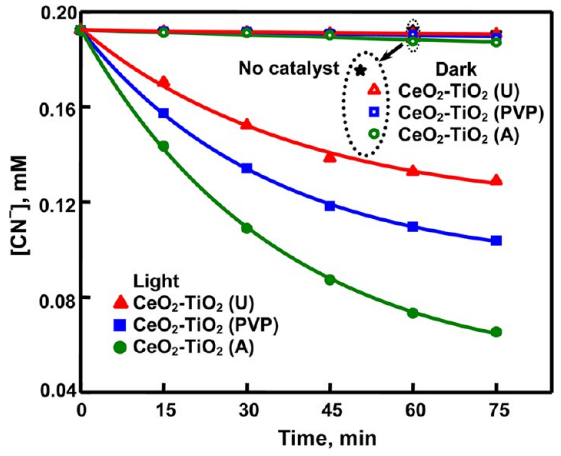

Figure 12. Visible light photocatalytic detoxification of cyanide: catalyst loading = 0.06 g, pH 12.5, airflow rate = 7.8 mL s^{-1}, $[O_2]_{dissolved}$ = 26.8 ppm, I = 1650 W m^{-2}, and volume of solution = 75 mL.

light of wavelengths between 320 and 400 nm. The adsorption of cyanide on the synthesized nanocomposites in dark under the experimental conditions is insignificant. As observed by earlier workers, photolysis under the experimental conditions (without photocatalyst) does not remove the cyanide ion significantly.

Formation of cyanate at the cost of cyanide was confirmed as stated elsewhere.[4] CeO_2−TiO_2 (A) is the most active photocatalyst to oxidize cyanide. The smallest particle size (<10 nm) and the largest visible light absorption range (<510 nm) are likely to be some of the reasons for the largest photocatalytic activity. But the photocatalytic activities of the other two composites are not in tune with their absorption edges. However, the observed photocatalytic activities are in agreement with the crystal size measured by TEM; the smaller is the crystal, the larger is the photocatalytic activity. To confirm the dependence of the photocatalytic activity on the particle size of the solvothermally synthesized CeO_2−TiO_2 nanocomposite, the photocatalytic detoxification of cyanide was carried out with UV A light (365 nm) of a mercury vapor lamp. Figure 13 displays the time profiles of cyanide oxidation photocatalyzed by the three synthesized nanocomposites. The temporal profiles show that CeO_2−TiO_2 (A) is more efficient than the other two nanocomposites to photocatalyze oxidation of cyanide. As the energy of illumination is larger than the band

dx.doi.org/10.1021/sc400195n | ACS Sustainable Chem. Eng. 2013, 1, 1555−1563

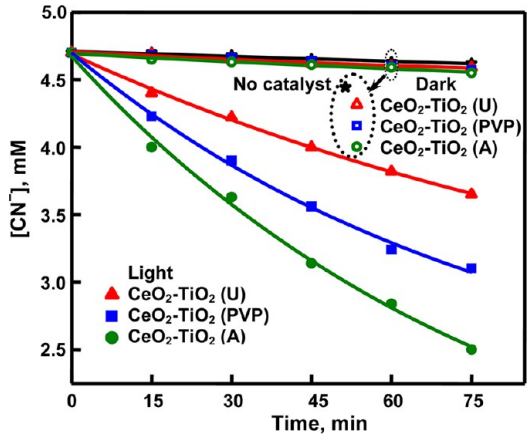

Figure 13. UV light photocatalytic detoxification of cyanide: catalyst loading = 0.02 g, pH 12.5, airflow rate = 7.8 mL s^{-1}, $[O_2]_{dissolved}$ = 26.8 ppm, λ = 365 nm, I = 25.4 μEinstein L^{-1} s^{-1}, and volume of solution = 25 mL.

gaps of the composites, it could be concluded that the particle size is having a large influence on photocatalytic activity. Figure 14 shows the reusability of the most active CeO_2−TiO_2 nanoparticulate photocatalyst under visible light.

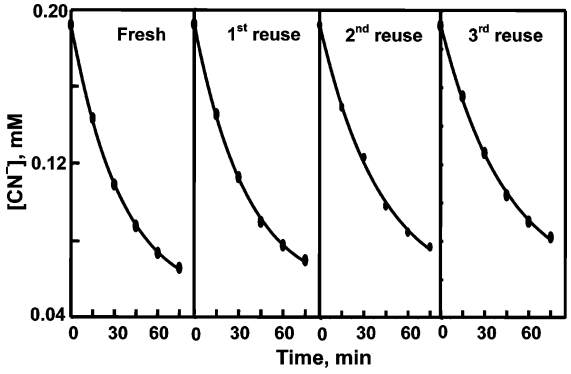

Figure 14. Reusability of CeO_2−TiO_2 (A) for visible light detoxification of cyanide, conditions as in Figure 12

Photocatalytic Degradation of Dye. Although recently many workers have reported synthesis of a photocatalyst to degrade a dye of their interest, no reason is given for the dye specificity in photocatalysis. Why is the proposed photocatalyst suited for the interested dye? An important characteristic of the reactive oxygen species such as the $HO^{\bullet}$ radical is its little selectivity of attack on a variety of organic molecules. Photocatalytic oxidation of cyanide by the three synthesized nanocomposites have been tested under a highly basic (pH 12.5) medium. To know the photocatalytic activity at neutral pH degradation of a dye has been examined under UV light; dye sensitization of the photocatalyst is less likely in photocatalysis by UV light. Figure 15 displays the degradation profiles of rhodamine B, a widely used dye to test photocatalytic activity, and the order of photocatalytic activity is the same as observed with cyanide in an alkaline medium. Hence, it is concluded that irrespective of pH the synthesized nanocomposites exhibit photocatalytic activity.

Bactericidal Activity. The bactericidal activity of the synthesized nanocomposites have been tested with methicillin-resistant *Staphylococcus aureus* (*S. aureus*), a Gram positive

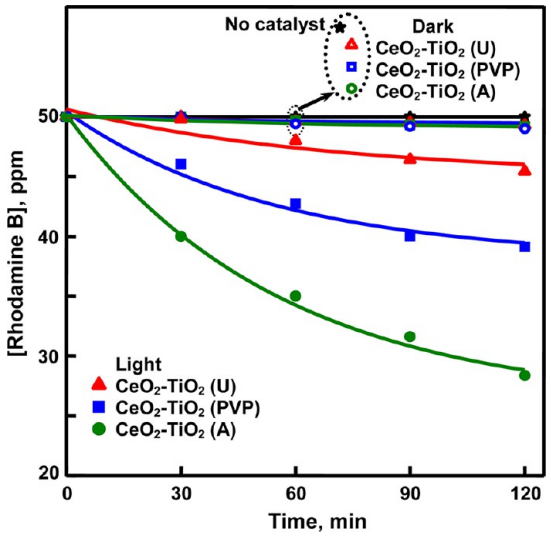

Figure 15. Photocatalytic degradation of dye: catalyst loading = 0.02 g, airflow rate = 7.8 mL s^{-1}, $[O_2]_{dissolved}$ = 26.8 ppm, λ = 365 nm, I = 25.4 μEinstein L^{-1} s^{-1}, and volume of solution = 25 mL.

bacteria. Figure 16 presents disinfection of *S. aureus* by the synthesized nanocomposites in aqueous suspension in the

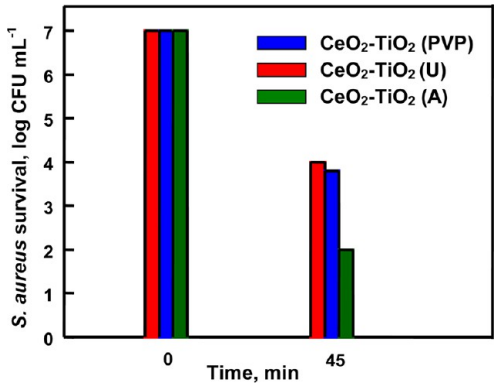

Figure 16. Inactification of *S. aureus*: composite loading = 0.02 g and volume of solution = 25 mL.

absence of illumination. The bacteria in 1.5% nutrient agar were used for the bactericidal study. The bactericidal test shows that CeO_2−TiO_2 (A) is a better bactericide than the other two. Here too, the smaller particle size may be a reason. A recent in vitro evaluation of the cytotoxicity of ZnO, CuO, Al_2O_3, La_2O_3, Fe_2O_3, SnO_2, and TiO_2 nanoparticles in terms of the LD_{50} of *E. coli*, after exposure to the listed oxides, shows that TiO_2 is the least toxic oxide, and ZnO is the most toxic one.[28] However, the present study shows that CeO_2−TiO_2 (A) exhibits significant bactericidal activity. Unlike ZnO, TiO_2 and CeO_2 are stable, and hence, the synthesized CeO_2−TiO_2 (A) is a promising visible light photocatalyst and bactericide. This is the first report of bactericidal activity by CeO_2−TiO_2, and the mechanism of bacteria inactivation is to be explored.

CONCLUSIONS

Ascorbic acid-, urea-, or polyvinylpyrrolidone-assisted solvothermally synthesized CeO_2−TiO_2 nanocomposites absorb visible light and photocatalyze detoxification of cyanide in alkaline medium. The CeO_2−TiO_2 nanocomposite synthesized

dx.doi.org/10.1021/sc400195n | ACS Sustainable Chem. Eng. 2013, 1, 1555−1563

using ascorbic acid is more efficient than the rest to photocatalytically detoxify cyanide. Of the three nanocomposites synthesized, the one obtained using ascorbic acid has the smallest particle size and largest visible light absorption window. The CeO_2−TiO_2 nanocomposites also photodegrade dye at neutral pH displaying nonspecificity of photocatalysis by the synthesized nanoparticles. The photocatalytic activities of the nanocomposites are commensurate with the particle sizes; the larger is the activity, the smaller is the particle size. The synthesized composites are bactericides as well.

AUTHOR INFORMATION

Corresponding Author

*E-mail: karunakaranc@rediffmail.com. Tel: +91 9443481590.

Notes

The authors declare no competing financial interest.

ACKNOWLEDGMENTS

The authors thank the Science and Engineering Research Board (SERB), Department of Science and Technology (DST), New Delhi, for the research project (SR/S1/PC-41/2011). Further, C.K. acknowledges the financial support from the Council of Scientific and Industrial Research (CSIR), New Delhi, under Scheme 21(0887)/12/EMR-II. P.G. thanks CSIR for the award of Senior Research Fellowship (SRF). The authors also thank Dr. J. Jayabharathi, Annamalai University, for the DRS and PL facilities.

REFERENCES

(1) Karunakaran, C. Semiconductor Catalyzed Photodetoxification of Cyanide. In *Photo/Electrochemistry & Photobiology in the Environment, Energy and Fuel*; Kaneco, S., Ed.; Research Signpost: Trivandrum, 2006.

(2) Marugan, J.; van Grieken, R.; Cassano, A. E.; Alfano, O. M. Scaling-up of slurry reactors for the photocatalytic oxidation of cyanide with TiO_2 and silica-supported TiO_2 suspensions. *Catal. Today* **2009**, *144*, 87−93.

(3) Marugan, J.; van Grieken, R.; Cassano, A. E.; Alfano, O. M. Intrinsic kinetic modeling with explicit radiation absorption effects of the photocatalytic oxidation of cyanide with TiO_2 and silica-supported TiO_2 suspensions. *Appl. Catal., B* **2008**, *85*, 48−60.

(4) Karunakaran, C.; Gomathisankar, P.; Manikandan, G. Preparation and characterization of antimicrobial Ce-doped ZnO nanoparticles for photocatalytic detoxification of cyanide. *Mater. Chem. Phys.* **2010**, *123*, 585−594.

(5) Karunakaran, C.; Abiramasundari, G.; Gomathisankar, P.; Manikandan, G.; Ananthi, V. Preparation and characterization of ZnO-TiO_2 nanocomposite for photocatalytic disinfection of bacteria and detoxification of cyanide under visible light. *Mater. Res. Bull.* **2011**, *46*, 1586−1592.

(6) Karunakaran, C.; Gomathisankar, P.; Manikandan, G. Solar photocatalytic detoxification of cyanide with bacterial disinfection by oxide ceramics. *Indian J. Chem. Technol.* **2011**, *18*, 169−176.

(7) Wang, P.; Cao, M.; Ao, Y.; Wang, C.; Hou, J.; Qian, J. Investigation on Ce-doped TiO_2-coated BDD composite electrode with high photoelectrocatalytic activity under visible light irradiation. *Electrochem. Commun.* **2011**, *13*, 1423−1426.

(8) Zou, M.; Kong, Y.; Wang, J.; Wang, Q.; Wang, Z.; Wang, B.; Fan, P. Spectroscopic analyses on ROS generation catalyzed by TiO_2, CeO_2/TiO_2 and Fe_2O_3/TiO_2 under ultrasonic and visible light irradiation. *Spectrochim. Acta, Part A* **2013**, *101*, 82−90.

(9) Ma, T.-Y.; Cao, J.-L.; Shao, G.-S.; Zhang, X.-J.; Yuan, Z.-Y. Hierarchically structured squama-like cerium-doped titania: Synthesis, photoactivity, and catalytic CO oxidation. *J. Phys. Chem. C* **2009**, *113*, 16658−16667.

(10) Magesh, G.; Viswanathan, B.; Viswanath, R. P.; Varadarajan, T. K. Photocatalytic behavior of CeO_2-TiO_2 system for the degradation of methylene blue. *Indian J. Chem. A* **2009**, *48*, 480−488.

(11) Xie, J.; Jiang, D.; Chen, M.; Li, D.; Zhu, J.; Lu, X.; Yan, C. Preparation and characterization of monodisperse Ce-doped TiO_2 microspheres with visible light photocatalytic activity. *Colloids Surf., A* **2010**, *372*, 107−114.

(12) Tong, T.; Zhang, J.; Tian, B.; Chen, F.; He, D.; Anpo, M. Preparation of Ce−TiO_2 catalysts by controlled hydrolysis of titanium alkoxide based on esterification reaction and study on its photocatalytic activity. *J. Colloid Interface Sci.* **2007**, *315*, 382−388.

(13) Liu, Y.; Fang, P.; Cheng, Y.; Gao, Y.; Chen, F.; Liu, Z.; Dai, Y. Study on enhanced photocatalytic performances of cerium doped TiO_2-based nanosheets. *Chem. Eng. J.* **2013**, *219*, 478−485.

(14) Stengl, V.; Bakardjieva, S.; Murafa, N. Preparation and photocatalytic activity of rare earth doped TiO_2 nanoparticles. *Mater. Chem. Phys.* **2009**, *114*, 217−226.

(15) Munoz-Batista, M. J.; Kubacka, A.; Gomez-Cerezo, M. N.; Tudela, D.; Fernandez-Garcia, M. Sunlight-driven toluene-elimination using CeO_2−TiO_2 composite systems: A kinetic study. *Appl. Catal., B* **2013**, *140−141*, 626−635.

(16) Rayner, J.; Zhang, H.; Schubert, J.; Lennon, P.; Lantagne, D.; Oyanedel-Craver, V. Laboratory investigation into the effect of silver application on the bacterial removal efficacy of filter material for use on locally produced ceramic water filters for household drinking water treatment. *ACS Sustainable Chem. Eng.* **2013**, *1*, 737−745.

(17) Wang, H.-F.; Chen, L.-Y.; Su, W.-N.; Chung, J.-C.; Hwang, B.-J. Effect of the compact TiO_2 layer on charge transfer between N3 dyes and TiO_2 investigated by Raman spectroscopy. *J. Phys. Chem. C* **2010**, *114*, 3185−3189.

(18) Wang, X.; Shen, J.; Pan, Q. Raman spectroscopy of sol-gel derived titanium oxide thin films. *J. Raman Spectrosc.* **2011**, *42*, 1578−1582.

(19) Zhang, Y.; Yuwono, A. H.; Wang, J.; Li, J. Enhanced photocatalysis by doping cerium into mesoporous titania thin films. *J. Phys. Chem. C* **2009**, *113*, 21406−21412.

(20) Zaharescu, M.; Wittmar, A.; Teodorescu, V.; Andronescu, C.; Wittmar, M.; Veith, M. TiO_2−CeO_2 nanometric powders prepared by sol-gel method. *Z. Anorg. Allg. Chem.* **2009**, *635*, 1915−1924.

(21) Taniguchi, T.; Watanabe, T.; Sugiyama, N.; Subramani, A. K.; Wagata, H.; Matsushita, N.; Yoshimura, M. Identifying defects in ceria-based nanocrystals by UV resonance Raman spectroscopy. *J. Phys. Chem. C* **2009**, *113*, 19789−19793.

(22) Li, G.-R.; Qu, D.-L.; Arurault, L.; Tong, Y.-X. Hierarchically porous Gd^{3+}-doped CeO_2 nanostructures for the remarkable enhancement of optical and magnetic properties. *J. Phys. Chem. C* **2009**, *113*, 1235−1241.

(23) Zhang, G.; Shen, Z.; Liu, M.; Guo, C.; Sun, P.; Yuan, Z.; Li, B.; Ding, D.; Chen, T. Synthesis and characterization of mesoporous ceria with hierarchical nanoarchitecture controlled by amino acids. *J. Phys. Chem. B* **2006**, *110*, 25782−25790.

(24) Zhang, Y.; Zhang, L.; Deng, J.; Dai, H.; He, H. Controlled synthesis, characterization, and morphology-dependent reducibility of ceria−zirconia−yttria solid solutions with nanorod-like, microspherical, microbowknot-like, and micro-octahedral shapes. *Inorg. Chem.* **2009**, *48*, 2181−2192.

(25) Wang, E.; Yang, W.; Cao, Y. Unique surface chemical species on indium doped TiO_2 and their effect on the visible light photocatalytic activity. *J. Phys. Chem. C* **2009**, *113*, 20912−20917.

(26) Maensiri, S.; Masingboon, C.; Laokul, P.; Jareonboon, W.; Promarak, V.; Anderson, P. L.; Seraphin, S. Egg white synthesis and photoluminescence of platelike clusters of CeO_2 nanoparticles. *Cryst. Growth Des.* **2007**, *7*, 950−955.

(27) Karunakaran, C.; Rajeswari, V.; Gomathisankar, P. Optical, electrical, photocatalytic, and bactericidal properties of microwave synthesized nanocrystalline Ag-ZnO and ZnO. *Solid State Sci.* **2011**, *13*, 923−928.

(28) Hu, X.; Cook, S.; Wang, P.; Hwang, H.-m. *In vitro* evaluation of cytotoxicity of engineered metal oxide nanoparticles. *Sci. Total Environ.* **2009**, *407*, 3070−3072.